IOPscience iopscience.iop.org

Home Search Collections Journals About Contact us My IOPscience

Effect of Surface Energy on Pentacene Thin-Film Growth and Organic Thin Film Transistor Characteristics

This content has been downloaded from IOPscience. Please scroll down to see the full text.

2009 Jpn. J. Appl. Phys. 48 031501

(http://iopscience.iop.org/1347-4065/48/3R/031501)

View the table of contents for this issue, or go to the journal homepage for more

Download details:

IP Address: 140.113.38.11

This content was downloaded on 25/04/2014 at 11:21

Please note that terms and conditions apply.

Effect of Surface Energy on Pentacene Thin-Film Growth and Organic Thin Film Transistor Characteristics

Hsiao-Wen Zan[1,2]* and Cheng-Wei Chou[2]

[1] *Department of Photonics and Display Institute, National Chiao Tung University, 1001 Ta-Hsueh Rd., Hsinchu 300, Taiwan*
[2] *Department of Photonics and Institute of Electro-Optical Engineering, National Chiao Tung University, 1001 Ta-Hsueh Rd., Hsinchu 300, Taiwan*

Received July 22, 2008; revised November 27, 2008; accepted December 6, 2008; published online March 23, 2009

In this study, we discuss pentacene-based organic thin films grown on a self-assembled monolayer (SAM)-treated dielectric with various functional groups and molecular lengths. The functional groups and molecular lengths on the dielectric surface were modified using a SAM treatment followed by ultra violet (UV) light exposure. Surface energy was used to observe the surface polarity variation during UV light exposure. After pentacene deposition, the growth modes of pentacene on surfaces with various surface characteristics were analyzed by atomic force microscope (AFM) and X-ray diffraction (XRD). The structure of pentacene growth on different surfaces with various surface characteristics was carefully examined. Organic thin film transistors fabricated with pentacene grown on various surfaces were characterized. When the polar components of surface energy were decreased, device mobility was increased from 0.04 to 0.21 $cm^2 V^{-1} s^{-1}$ and the threshold voltage shifted from −13.55 to −3.2 V. © 2009 The Japan Society of Applied Physics

DOI: 10.1143/JJAP.48.031501

1. Introduction

In recent years, pentacene-based organic molecular semiconductors have been commonly used to fabricate active elements in optoelectronic devices owing to their low processing temperature and low cost.[1–4] The electrical characteristics of the devices were dominated by the interface between the pentacene film and the gate dielectric.[5,6] Interface properties such as roughness, functional groups, and surface energy were observed to affect the organic film growth.[7–13] The ordering of the molecular structure and crystallization of an organic thin film have been proven to be significant factors in determining device performance.[14–16] Numerous studies have been performed to effectively modify the gate dielectric surface to improve the ordering of the pentacene molecules.[16–21] Many surface treatment methods have been proposed to effectively modify the gate dielectric surface to improve the electrical characteristics of the device. For example, a self-assembled monolayer (SAM) was used as a modifying layer between the silicon oxide (SiO_2) gate dielectric and the pentacene layer to improve charge transport in the device.[19,20] Kelley *et al.* found that mobility in the organic thin film transistors (OTFTs) could be increased to 3 $cm^2 V^{-1} s^{-1}$ using an alumina gate dielectric treated with SAM-alkylphosphonic acid.[22] To obtain high-performance pentacene-based OTFTs, SAM was an important component in pentacene growth.

Sugimura *et al.* proposed that SAM could be destroyed, layer by layer, by ultraviolet (UV) exposure.[23] During UV exposure, some polar functional groups such as –CHO and –COOH are formed. The mechanism of pentacene growth on different layers of SAM with different functional groups and different molecular lengths are discussed in this study. The SAM material octadecyltrimethoxysilane (ODMS) was exposed to UV (wavelength: 175–285 nm) light for varying times to destroy the organic film layer by layer. The functional groups and the molecular lengths were changed as a function of UV light exposure time. The surface morphology and crystalline structures of pentacene films were varied when they were deposited on various surfaces at different UV exposure times. Using this simple and convenient method, the pentacene growth modes and characteristics were controlled and demonstrated in this study.

2. Experiments

2.1 Device fabrication and procedures

Heavily doped n-type Si(100) wafers with a 1000-Å-thick SiO_2 layer were used as substrates. Before the surface of the SiO_2 was treated with ODMS solution, the samples were cleaned with acetone, isopropanol, and acetone solution in that order. Then, the sample was dipped in dissolved ODMS to make the surface of the silicon oxide hydrophobic. The concentration of ODMS was 10 mM. Next, the surfaces were exposed to UV light (wavelength: 175–285 nm, power: 40 mW, dose: 0.043 mW/cm^2) for times varying from 0 to 30 min. The UV exposure process was carried out in a non vacuum chamber (in air). As shown in Fig. 1(a), the contact angle and the surface energy were controlled by the duration of exposure to UV light. The pentacene was deposited by thermal evaporation and was defined through a shadow mask onto ODMS regions, followed by UV exposure. The thickness of the pentacene film was approximately 100 nm and the deposition rate was ~0.5 Å/s. Finally, 100-nm-thick Au pads were deposited through a shadow mask as source/drain contacts, and the device channel width and length were defined as 600 and 200 μm, respectively. To serve as a control, OTFTs fabricated by a conventional process without ODMS treatment or UV light exposure were labeled as conventional devices.

2.2 Characterization

Contact angle measurements were used to study the composition of hydrophobic and hydrophilic functional groups. The water contact angle was sensitive to the chemical composition of the film surface. The contact angle was obtained using a Krüss contact angle system for universal surface testing (model GH-100). The contact angles of three standard liquids (de-ionized water, diiodo

*E-mail address: hsiaowen@mail.nctu.edu.tw

 © 2009 The Japan Society of Applied Physics

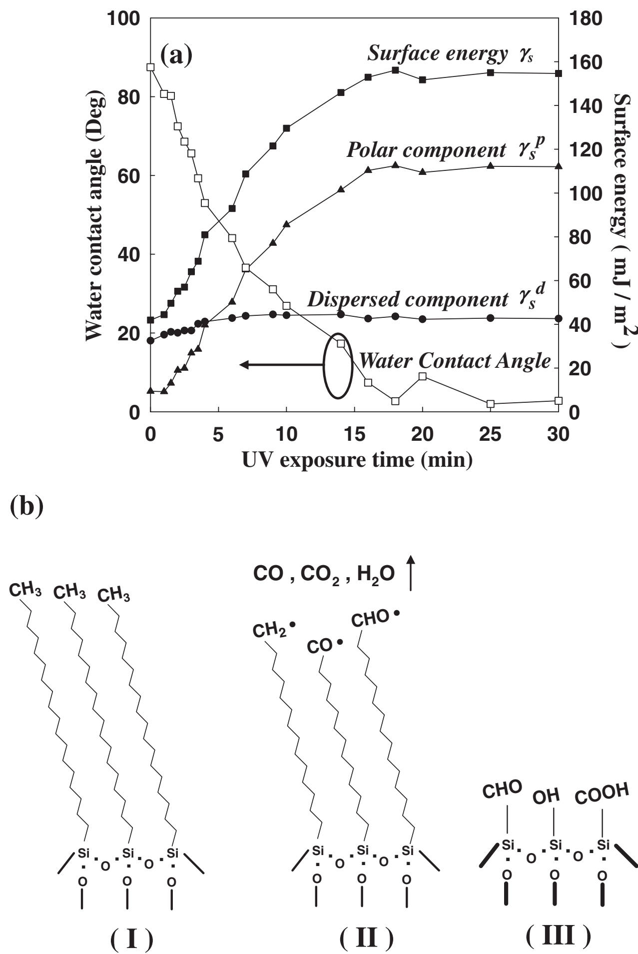

Fig. 1. (a) Effect of UV light exposure time on the surface contact angle and the surface energy following ODMS treatment. The open symbols represent the water contact angle. The solid squares represent the surface energy (γ_S) calculated from the contact angle. The solid circles and triangles are the dispersed component γ_S^d and polar component γ_S^p of surface energy. (b) Schematic shows the chemical bonds modified during UV light exposure.

methane, and ethylene glycol) were measured to determine the surface energy of the material. Variation in the contact angle represents a change in surface energy. Surface energy was calculated using Fowkes and Young's approximation, as[24,25)]

$$(1 + \cos\theta)\gamma_L = 2(\gamma_S^d \gamma_L^d)^{1/2} + 2(\gamma_S^p \gamma_L^p)^{1/2}, \tag{1}$$

where θ is the measured contact angle; γ_L is the surface energy of the tested liquid, which is the sum of its dispersed part γ_L^d and its polar part γ_L^p. γ_S^d and γ_S^p are the dispersion and polar components, respectively, of the surface energy of the solid surface. The total surface energy of the solid γ_S can be estimated as

$$\gamma_S \cong \gamma_S^p + \gamma_S^d. \tag{2}$$

The surface composition and chemical bonding states were investigated by X-ray photoelectron spectroscopy (XPS; ESCA PHI1600). X-ray radiation was provided by a monochromated Mg anode Kα line at 1253.6 eV. The base pressure of the instrument was 6.67×10^{-7} Pa. The C 1s signal at 284.5 eV was used as a reference for all peak positions. To separate chemical bonding states in the XPS spectra, the spectral line shape was simulated using a suitable combination of Gaussian and Lorentzian functions.

All the electrical characteristics were measured in this work using Agilent 4156 and 4284 analyzers. The field-effect mobility and threshold voltage were calculated from the slope and the intercept of the square root of the I_D vs V_G plot. The interface state density was determined by the method proposed in ref. 26.

$$N_{SS} = \left(\frac{S \log e}{kT/q} - 1\right)\frac{C_i}{q}, \tag{3}$$

where q is the electron charge, S is the subthreshold swing, T is the temperature, k is the Boltzmann constant, and C_i is the insulator capacitance per unit area.

3. Results and Discussion

3.1 Contact angle and surface composition analysis

As shown in Fig. 1(a), the open symbols represent the water contact angle on the dielectric surface. The water contact angle on bare SiO_2 was approximately 48.5° before any treatment. The water contact angle of the SiO_2 surface treated with ODMS solution was altered to about 90°. The water contact angle variation indicates that the SiO_2 surface was apparently transformed from hydrophilic to hydrophobic by the ODMS solution. Following exposure to UV light, the contact angle changed rapidly with time. During a 25 min UV light exposure, the water contact angle changed by approximately 90°. Figure 1(a) is also a plot of the calculated results for γ_S^d, γ_S^p, and γ_S. The solid squares represent the surface energy (γ_S) calculated from the contact angle. The solid circles and triangles represent the dispersed component γ_S^d and polar component γ_S^p of surface energy. The surface energy γ_S increased as the water contact angle decreased.

Figure 1(b) is a schematic of the ODMS surface characteristics during UV light exposure. Chemical bonds such as C–C, C–H, and C–Si were decomposed by UV light and the radicals shown in Fig. 1(b) were formed.[23)] Such radicals may further react with oxygen and water molecules in the atmosphere. As shown in Fig. 1(b-II) and 1(b-III), polar functional groups such as –CHO and –COOH were formed during UV light exposure. The contact angle was altered when the chemical bonds were excited to form polar functional groups. After 30 min of exposure, the organic film (ODMS) and the surface polarity were efficiently destroyed by UV light.[23)] These results were consistent with the polar components of the surface energy γ_S^p increasing with UV exposure time. Most likely, the increased polar components of the surface energy γ_S^p were due to polar functional groups such as CHO and COOH formed during UV light exposure.[18,23)]

To understand the surface chemistry of samples after UV exposure, samples were characterized by XPS. The XPS spectra of the C 1s core level from surfaces treated with UV light for various times are shown in Figs. 2(a)–2(c). The curve-fit data in Figs. 2(a)–2(c) indicate that the C 1s signal consists of a C–C peak at 284.5 eV, a C–O peak at 286.7 eV, and an O–C=O peak at 288.5 eV.[27–29)] A decreased C–C peak intensity ratio was observed for the surfaces treated with UV light. The decreased C 1s peak at 284.5 eV indicated the decrease of C–C bonds, and the decomposition

 © 2009 The Japan Society of Applied Physics

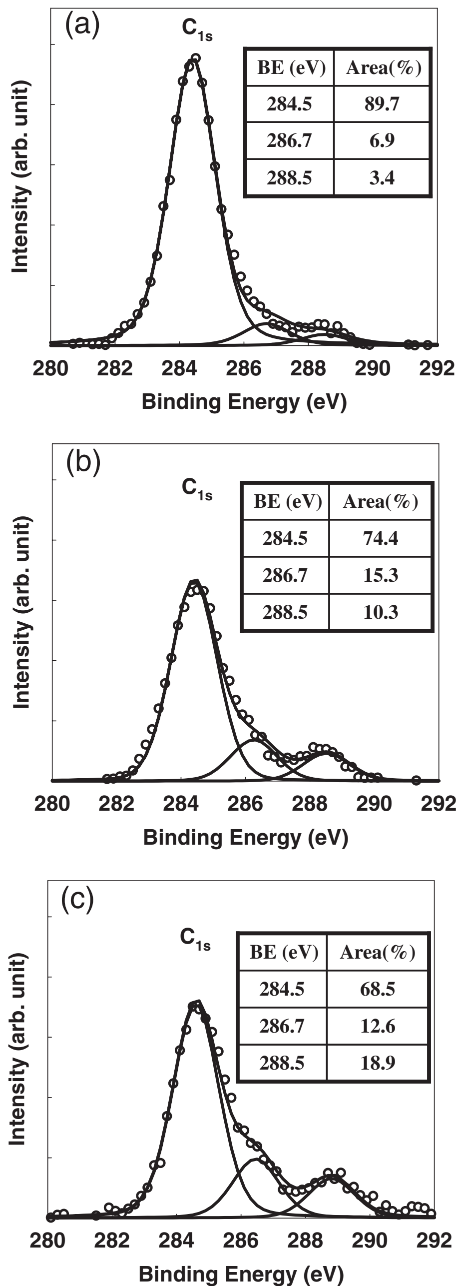

BE (eV)	Area(%)
284.5	89.7
286.7	6.9
288.5	3.4

BE (eV)	Area(%)
284.5	74.4
286.7	15.3
288.5	10.3

BE (eV)	Area(%)
284.5	68.5
286.7	12.6
288.5	18.9

Fig. 2. XPS spectra of C 1s core levels from the surface after (a) no UV exposure, (b) 15 min UV exposure, and (c) 30 min UV exposure. The binding energy (BE) position and peak area of the curve-fit data are listed in the inserted tables.

of ODMS. Decomposed ODMS on the SiO_2 surface made the surface hydrophilic and increased the surface energy.

After the ODMS was exposed to UV light, the signals due to oxidized carbon components, C–O and O–C=O, increased. This observation agreed with the increased polar component of the surface energy at longer UV exposure times, as shown in Fig. 1(a). The increased surface energy was thus attributed to the destruction of C–C bonds and an increase in the relative amounts of C–O and O–C=O bonds on the SiO_2 surface. The increased signals due to oxidized carbon components were also consistent with the schematic of ODMS decomposition shown in Fig. 1(b). After UV exposure, ODMS on the SiO_2 surface was oxidized and polar functional groups were generated.

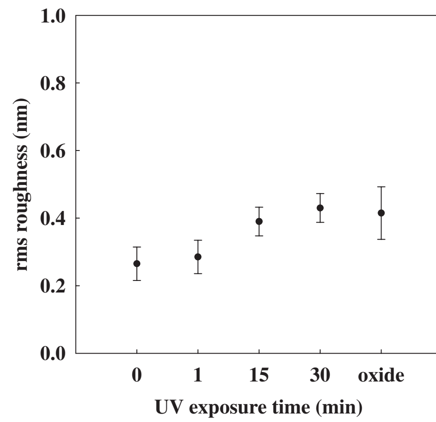

Fig. 3. Plot of roughness vs UV exposure time of the ODMS-treated substrate.

3.2 Roughness analysis

After UV exposure, the surface polarity and surface energy of the ODMS-treated SiO_2 surface increased. The destroyed organic surface showed a roughened topography.[18,30–33] Pentacene grown on a dielectric surface affected by surface roughness has been previously reported.[7–11,18] As shown in Fig. 3, the surface roughness of bare SiO_2 and ODMS-treated SiO_2 following various UV exposure times were compared. The surface roughness was measured by tapping mode atomic force microscopy (AFM; Digital Instrument Dimension 3100). The error bars were calculated from data collected from three different regions with identical $3 \times 3\,\mu m^2$ areas. The SiO_2 surface treated with ODMS solution showed reduced surface roughness and increased surface uniformity. Under UV exposure, the surface roughness increased with increasing exposure time. However, variations in the organic molecular surface roughness had little effect on subsequent deposits of pentacene, as proposed by Shin *et al.*[11] Compared to Shin *et al.*, the roughness variation ($\sim$0.2 nm) was less than 0.31 nm and had little effect on pentacene growth.

3.3 Pentacene growth analysis

Figure 4 shows the AFM images of 1000-Å-thick pentacene film deposited on regions with varying surface-treatment conditions. Figure 4(a) is the pentacene deposited on a SiO_2 surface treated with ODMS solution. AFM images of the pentacene films deposited on the SiO_2 surface, which were treated with ODMS solution followed by UV exposure for 1, 15, and 30 min, are shown in Figs. 4(b)–4(d). The conventional device shown in Fig. 4(e) was pentacene deposited on bare SiO_2 without any treatment. The AFM images indicate that the pentacene morphology on the non UV-exposed samples [Fig. 4(a)] had smaller grains than that on the UV-exposed samples [Figs. 4(b)–4(d)]. Large and dendritic grains were observed for pentacene in Figs. 4(d) and 4(e). These grain structures grow using the Stranski–Krastanov growth mode (two-dimensional growth).[34] Yang *et al.* proposed that the pentacene film deposited on a surface with a high surface energy would have a large grain size.[13] Surface energy increased with UV exposure time in this work. The grain size was enlarged when pentacene film was deposited on a surface with a high surface energy. When

 © 2009 The Japan Society of Applied Physics

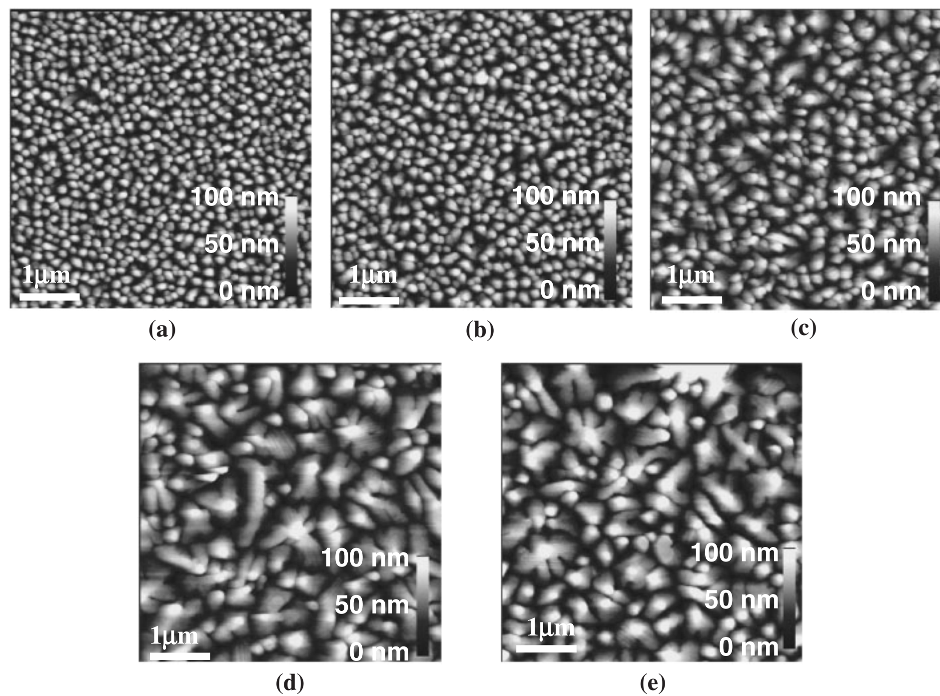

Fig. 4. AFM images of the pentacene film deposited on surfaces with (a) no UV exposure, (b) 1 min UV exposure, (c) 15 min UV exposure, and (d) 30 min UV exposure to regions of ODMS-treated substrate, and (e) conventional substrate (SiO_2 substrate without ODMS treatment). The nonlinear *z*-axis scale is shown in the AFM images.

pentacene was deposited on the substrates exposed to UV for 1 and 15 min [Figs. 4(b) and 4(c)], the pentacene grain growth was affected by surface energy variation. The modified surface energy and pentacene growth mode were due to the changes in functional groups, such as $–CH_2$, $–CH_3$, –CHO, –COOH, and –OH. The AFM images shown in Figs. 4(b) and 4(c) reveal disordered pentacene morphology. In Fig. 4(c), some small pentacene grains were mixed among the dendritic grains. Disordered pentacene grains were also observed in Fig. 4(b).

As shown in Fig. 5, X-ray diffraction (XRD) was used to observe pentacene growth and crystallization on various surfaces. XRD patterns were obtained using Cu Kα radiation ($\lambda_{K\alpha 1} = 1.5406$ Å) and measured in the symmetric diffraction coupled θ–2θ mode. The structures of 1000-Å-thick pentacene films shown in Figs. 4(a)–4(e) were measured by XRD at room temperature in ambient air. The presence of only a (00*l*) reflection and the absence of any other (*hkl*) reflections indicate that all the crystals in the film are oriented with their (00*l*) planes parallel to the substrate. Two distinct crystalline phases, a "thin-film phase" and a "single-crystal phase",[17,35,36] with corresponding d_{001}-spacings of 15.4 and 14.5 Å are usually observed in the θ–2θ patterns of the XRD spectra of pentacene. The pentacene film grown on a surface treated with ODMS solution followed by several minutes of UV exposure also showed two crystalline phases. However, the pentacene film deposited on a SiO_2 surface treated with ODMS solution without UV exposure had only one crystalline phase, the thin film phase, and a sharp first-order diffraction peak. Obviously, pentacene grown on an ODMS-treated surface with its sharp diffraction peak and high peak intensity is a better quality of crystal than that grown on a bare SiO_2 surface.[17] Pentacene film grown on a surface with various surface energies had different growth modes. These growth modes may lead to different crystalline phases. When the pentacene film was grown on a surface with a low surface energy, the pentacene growth was dominated by the Volmer–Weber growth mode. Pentacene film grown on the surface treated with ODMS without UV light exposure had a single crystal phase in the XRD patterns (Fig. 5) owing to the single growth mode. When the pentacene film was grown on a surface with a high surface energy, the Stranski–Krastanov growth mode started to combine with the pentacene growth. The mixed pentacene growth modes resulted in multiple crystal phases. In addition to the mixed growth modes in the crystal phase, the bulk phase shown in Fig. 5 was also possible due to the enlarged crystal grains. Yanagisawa *et al.* reported the possibility that the bulk phase observed in XRD spectra was located at the defective (recessed) part in a large crystal pentacene grain.[37] The recessed region extended across the pentacene molecular steps without perturbing the step continuity. The recessed parts in pentacene morphology reported by Yanagisawa *et al.* were also visible in Figs. 4(d) and 4(e). This observation may indicate one of the origins of the pentacene growth on a high surface energy dielectric presenting two crystal phases. As a result of the XRD spectra shown in Fig. 5, the disordered pentacene crystal phase was observed on the surface treated by UV light (high surface energy), and the quality of pentacene crystals decreased with increasing UV exposure time.

3.4 Device characteristics

The electrical characteristics confirmed that the penatcene was modified when the quality of the pentacene crystalline structure varied with UV light exposure. Figure 6(a) is a comparison of the transfer characteristics of OTFTs under different conditions. Table I lists typical parameters such as

 © 2009 The Japan Society of Applied Physics

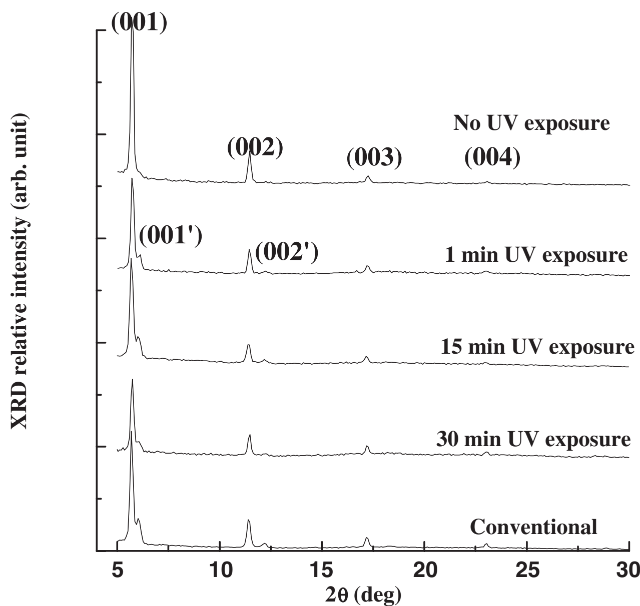

Fig. 5. XRD patterns of 1000-Å-thick pentacene film grown on regions of ODMS-treated substrate without UV exposure, and with 1, 15, and 30 min UV exposure and on conventional substrate (SiO_2 substrate without ODMS treatment).

mobility, threshold voltage, on/off current ratio, sub threshold swing, and the extracted interface state density (N_{SS}).

The ODMS-treated OTFT markedly outperformed conventional devices without ODMS treatment. A steep subthreshold characteristic (SS), a high field-effect mobility (μ_{FE}) of the saturation region, and a low interface trap density (N_{SS}) were obtained. It was reported that voids and successive, incomplete layers over the first pentacene layer were reduced when pentacene was deposited on a gate dielectric with nonpolar functional groups. The reduced voids in the incomplete layers help carrier transport and increase the carrier mobility.[17] As shown in Fig. 1(a), the polar component γ_S^p of the surface energy was reduced when the SiO_2 surface was treated with ODMS solution. Mobility decreased with UV exposure time and an increasing polar component surface energy γ_S^p. Otherwise, the mobility was lower than that of the conventional device when a long UV exposure time was used to treat the surface of the ODMS-treated SiO_2. The decrease in mobility may be partly caused by the high energy and long UV light exposure time which damaged the bare SiO_2 surface and formed extra defects, which affected carrier transport.

The magnitude of interface state density N_{SS} for OTFTs fabricated on the ODMS-treated SiO_2 surface was lower than for those fabricated on bare SiO_2. The lower interface state density in ODMS-treated SiO_2 was due to interface states on bare SiO_2 surfaces passivated by the ODMS solution. Compared with conventional samples, a larger trap state density was observed for OTFTs fabricated on the ODMS-treated SiO_2 followed by a long UV exposure time ($\sim$15 min). These results were consistent with the results for mobility. Extra defect states may be created during a long exposure to UV light. The increased traps may be attributed to the increased polar groups and the increased surface roughness after UV exposure of the dielectric surface. ODMS after UV exposure was decomposed layer by layer

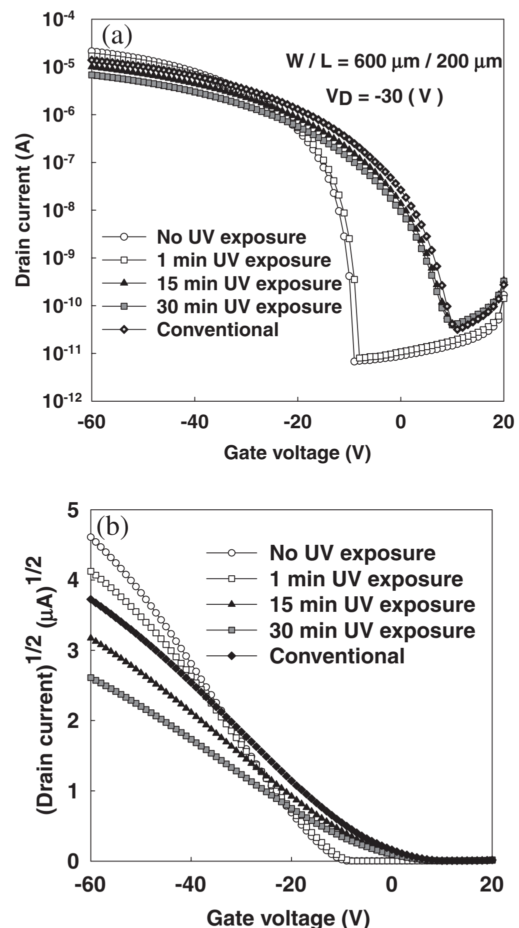

Fig. 6. (a) Transfer characteristics of various OTFTs fabricated on ODMS-treated substrate. Conventional devices were OTFTs without any ODMS treatment or UV exposure. The devices with no UV exposure were OTFTs fabricated on ODMS-treated substrates. The UV exposed samples were pentacene deposited onto the dielectric after ODMS treatment with various UV exposure times; (b) the square roots of the I_D vs V_G plot for the respective samples.

Table I. Calculated parameters of OTFTs under various conditions.

	No UV exposure	1 min UV exposure	15 min UV exposure	30 min UV exposure	Conventional
μ_{FE} ($cm^2 V^{-1} s^{-1}$)	0.21	0.16	0.06	0.04	0.09
V_{TH} (V)	−13.55	−11.68	−3.48	−3.2	−2.59
I_{on}/I_{off}	$>10^6$	$>10^5$	$<10^5$	$<10^5$	$\sim10^5$
SS (V/dec)	0.76	0.8	3.08	3.39	2.67
N_{SS} ($cm^{-2} eV^{-1}$)	2.53×10^{12}	2.68×10^{12}	1.09×10^{13}	1.2×10^{13}	9.4×10^{12}

during UV exposure. The functional group after UV exposure was oxidized, as shown in Fig. 1(b-II), and the polar groups was increased. Polar groups at the organic/insulator interface possibly formed deeper polaronic states. Stassen *et al.* reported that a higher polaronic organic/insulator interface generated a higher electrostatic potential. An attractive force on the charge carrier exerted by the enhanced electrostatic potential increased the tendency toward carrier self-trapping.[38] It is possible that the carrier self-trapping was one of the reasons for the increased trap density. Moreover, the slightly increased surface roughness

© 2009 The Japan Society of Applied Physics

may also be one of the origins of the increased trap density. A dielectric with poor surface roughness leads to valleys in the channel region. These valleys act as carrier traps with a number of scatterings and lead to increased trap density.[39)]

In addition, the threshold voltages of OTFTs fabricated on various surfaces were also varied. Threshold voltage, off current, and *SS* value were roughly classified into two groups, as shown in Fig 6. Group A (OTFTs fabricated on samples without UV exposure and on those with 1 min UV exposure) had low I_{off} and low *SS*. Group B (OTFTs fabricated on samples with 15 min UV exposure and on those with 30 min UV exposure) had inferior characteristics compared with Group A. This difference in threshold voltage may be due to the variation in surface energy. Surface energy increased rapidly when UV exposure time was increased from 1 to 15 min. After 15 min UV exposure, the surface energy remained almost unchanged with increasing UV exposure time. The surface energy was also roughly classified into two groups. The samples without UV exposure and with 1 min UV exposure had a similar low surface energy of 22 mJ/m^2, while the samples with 15 and 30 min UV exposure had a similar high surface energy of 83 mJ/m^2. The former corresponds to the good transfer characteristics of Group A devices; the latter corresponds to the inferior transfer performance of Group B devices. The modified surface energy was affected by changes in thickness, ordering, and surface chemical composition.

4. Conclusions

Pentacene films grown on SiO_2 surfaces treated with ODMS and various UV exposure times were characterized by AFM, XRD, and OTFT. Clear connections among surface energy, pentacene morphology, pentacene crystalline structure, the corresponding film growth mode, and carrier mobility were established. The pentacene structure and electrical characteristics were controlled by UV exposure time in this study. The pentacene growth mode was controlled from three-dimensional growth to two-dimensional growth by increasing UV exposure time. The morphology of 1000-Å-thick pentacene films was modified from small grains to large and dendritic-like grains. The field effect mobility was also modified by UV light exposure time from 0.21 to 0.04 $cm^2 V^{-1} s^{-1}$. The proposed method is a convenient and simple means to observe pentacene growth and its corresponding characteristics for further OTFT research.

Acknowledgements

The authors thank Professor Jenn-Chang Hwang at the Materials Science and Engineering Institute, NTHU, and Mr. H. T. Song at the Display Institute, NCTU, for their support in XPS analysis and film deposition. The authors are grateful to the National Center for High-performance Computing for computer time and facilities. This work was funded through the National Science Council of the Republic of China (Contract no. NSC 96-2221-E-009-127-MY2) and the National Nano Device Laboratories (Contract no. P96-1A-021).

1) S. F. Nelson, Y.-Y. Lin, D. J. Gundlach, and T. N. Jackson: Appl. Phys. Lett. **72** (1998) 1854.
2) C. Goldmann, S. Haas, C. Krellner, K. P. Pernstich, D. J. Gundlach, and B. Batlogg: J. Appl. Phys. **96** (2004) 2080.
3) H.-W. Zan, K.-H. Yen, P.-K. Liu, K.-H. Ku, C.-H. Chen, and J. Hwang: Jpn. J. Appl. Phys. **45** (2006) L1093.
4) H. L. Cheng, W. Y. Chou, C. W. Kuo, Y. S. Mai, F. C. Tang, and S. H. Lai: Proc. SPIE **6336** (2006) 63361B.
5) I. Yagi, K. Tsukagoshi, and Y. Aoyagi: Appl. Phys. Lett. **86** (2005) 103502.
6) H. W. Zan, K. H. Yen, C. H. Chen, P. K. Liu, K. H. Ku, and J. C. Hwang: Electrochem. Solid-State Lett. **10** (2007) H8.
7) D. Knipp, R. A. Street, and A. R. Völkel: Appl. Phys. Lett. **82** (2003) 3907.
8) D. Knipp, R. A. Street, A. R. Völkel, and J. Ho: J. Appl. Phys. **93** (2003) 347.
9) S. Steudel, S. D. Vusser, S. D. Jonge, D. Janssen, S. Verlaak, J. Genoe, and P. Heremans: Appl. Phys. Lett. **85** (2004) 4400.
10) S. E. Fritz, T. W. Kelley, and C. D. Frisbie: J. Phys. Chem. B **109** (2005) 10574.
11) K. Shin, C. Yang, S. Y. Yang, H. Jean, and C. E. Park: Appl. Phys. Lett. **88** (2006) 072109.
12) Y. Jang, J. H. Cho, D. H. Kim, Y. D. Park, M. Hwang, and K. Cho: Appl. Phys. Lett. **90** (2007) 132104.
13) S. Y. Yang, K. Shin, and C. E. Park: Adv. Funct. Mater. **15** (2005) 1806.
14) D. J. Gundlach, Y. Y. Lin, T. N. Jackson, S. F. Nelson, and D. G. Schlom: IEEE Electron Device Lett. **18** (1997) 87.
15) H. Sirringhaus, P. L. Brown, R. H. Friend, M. M. Nielsen, K. Bechgaard, B. M. W. Langeveld-Voss, A. J. H. Spiering, R. A. J. Janssen, E. W. Meijer, P. Herwig, and D. M. de Leeuw: Nature **401** (1999) 685.
16) W. Y. Chou and H. L. Cheng: Adv. Funct. Mater. **14** (2004) 811.
17) W. Y. Chou, C. W. Kuo, H. L. Cheng, Y. S. Mai, F. C. Tang, S. T. Lin, C. Y. Yeh, J. B. Horng, C. T. Chia, C. C. Liao, and D. Y. Shu: J. Appl. Phys. **99** (2006) 114511.
18) K. Shin, S. Y. Yang, C. Yang, H. Jeon, and C. E. Park: Org. Electron. **8** (2007) 336.
19) M. McDowell, I. G. Hill, J. E. McDermott, S. L. Bernasek, and J. Schwartz: Appl. Phys. Lett. **88** (2006) 073505.
20) A. Inoue, T. Ishida, N. Choi, W. Mizutani, and H. Tokumoto: Appl. Phys. Lett. **73** (1998) 1976.
21) C. Kim, A. Facchetti, and T. J. Marks: Adv. Mater. **19** (2007) 2561.
22) T. W. Kelley, L. D. Boardman, T. D. Dunbar, D. V. Muyres, M. J. Pellerite, and T. P. Smith: J. Phys. Chem. B **107** (2003) 5877.
23) H. Sugimura, N. Saito, Y. Ishida, I. Ikeda, K. Hayashi, and O. Takai: J. Vac. Sci. Technol. A **22** (2004) 1428.
24) D. Myers: *Surfaces, Interfaces, and Colloids: Principles and Applications* (Wiley, New York, 1999) 2nd ed., p. 430.
25) F. M. Fowkes: J. Phys. Chem. **67** (1963) 2538.
26) K. N. Narayanan Unni, S. Dabos-Seignon, and J.-M. Nunzi: J. Phys. D **38** (2005) 1148.
27) A. Zhu, M. Zhang, J. Wu, and J. Shen: Biomaterials **23** (2002) 4657.
28) G. J. Fleming, K. Adib, J. A. Rodriguez, M. A. Barteau, J. M. White, and H. Idriss: Surf. Sci. **602** (2008) 2029.
29) A. M. Shanmugharaj, S. Sabharwal, A. B. Majali, V. K. Tikku, and A. K. Bhowmick: J. Mater. Sci. **37** (2002) 2781.
30) C. Jinan, L. Fuzhi, L. Baoming, and Y. K. Daniel: Langmuir **20** (2004) 10919.
31) M. R. Sanchis, V. Blanes, M. Blanes, D. Garcia, and R. Balart: Eur. Polym. J. **42** (2006) 1558.
32) L. Carrino, W. Polini, and L. Sorrentino: J. Mater. Process. Technol. **153–154** (2004) 519.
33) K. S. Kim, C. M. Ryu, C. S. Park, G. S. Sur, and C. E. Park: Polymer **44** (2003) 6287.
34) D. L. Smith: *Thin-Film Deposition: Principles and Practice* (McGraw-Hill, New York, 1995) Chap. 5.
35) R. B. Campbell, J. Monteath Robertson, and J. Trotter: Acta Crystallogr. **14** (1961) 705.
36) C. D. Dimitrakopoulos and A. Pomp: J. Appl. Phys. **80** (1996) 2501.
37) H. Yanagisawa, T. Tamaki, M. Nakamura, and K. Kudo: Thin Solid Films **464** (2004) 398.
38) A. F. Stassen, R. W. I. de Boer, N. N. Losad, and A. F. Morpurgo: Appl. Phys. Lett. **85** (2004) 3899.
39) J. H. Kwon, J. H. Seo, S. I. Shin, K. H. Kim, D. H. Choi, I. B. Kang, H. Kang, and B. K. Ju: IEEE Trans. Electron Devices **55** (2008) 500.

© 2009 The Japan Society of Applied Physics